Climate
of the Past
Discussions

Open Access

EGU

1

Comparison of Cenozoic surface uplift and glacial-interglacial cycles on Himalaya-Tibet paleo-climate: Insights from a regional climate model

6
7
8
9
10
11

Heiko Paeth[1]*
Christian Steger[1,2]
Jingmin Li[3,4]
Sebastian G. Mutz[3]
Todd A. Ehlers[3]

17
18
19
20
21

[1] Institute of Geography and Geology, University of Würzburg, Germany
[2] now at: Deutscher Wetterdienst, Offenbach, Germany
[3] Department of Geosciences, University of Tübingen, Germany
[4] now at: Institute of Geography and Geology, Univ. of Würzburg, Germany

26
27
28
29
30
31
32
33
34

* Corresponding author:

Institute of Geography and Geology
University of Würzburg
Am Hubland
97070 Würzburg, Germany
Tel.: +49 931 3184688
Fax: +49 931 3185544
heiko.paeth@uni-wuerzburg.de

43

Climate
of the Past
Discussions

Open Access

EGU

Abstract

46 Assessing paleo-climatic changes across the Tibetan Plateau and the underlying

47 driving mechanisms provides insights for the natural variability in the Earth's climate

48 system in response to tectonic processes and global climate change. In this study, we

49 use a high-resolution regional climate model to investigate various episodes of distinct

50 climate states over the Tibetan Plateau region during the Cenozoic rise of the Plateau

51 and Quaternary glacial/interglacial cycles. The main objective is to compare climate

52 changes during the Miocene-Pliocene uplift period with climate anomalies during the

53 last glacial maximum and the mid-Holocene optimum, based on a consistent modeling

54 framework.

55 Reduced plateau elevation leads to regionally differentiated patterns of higher

56 temperature and lower precipitation amount on the plateau itself, whereas surrounding

57 regions are subject to colder conditions. In particular, Central Asia receives much more

58 precipitation prior to the uplift, mainly due to a shift of the stationary wave train over

59 Eurasia. Cluster analysis indicates that the continental-desert type climate, which is

60 widespread over Central Asia today, appears with the Tibetan Plateau reaching 50 %

61 of its present-day elevation.

62 The mid-Holocene is characterized by slightly colder temperatures, and the last glacial

63 maximum by considerably colder conditions over most of central and southern Asia.

64 Precipitation anomalies during these episodes are less pronounced and spatially

65 heterogeneous over the Tibetan Plateau. The simulated changes are in good

66 agreement with available paleo-climatic reconstructions from proxy data. The present-

67 day climate classification is only slightly sensitive to the changed boundary conditions

68 in the Quaternary Quaternary. It is shown that in some regions of the Tibetan Plateau

69   the climate anomalies during the Quaternary Quaternary have been as strong as the

70   changes occurring during the uplift period.

71

72   **Keywords:** Tibetan Plateau, dynamical downscaling, paleo-climate, surface uplift,

73   Last Glacial Maximum, mid-Holocene

74

1 Introduction

The Tibetan Plateau (TP) is the highest and largest modern elevated plateau and a primary feature of Earth's climate system. Over the last millions of years it has undergone remarkable climate changes, especially during the Miocene-Pliocene uplift period (Clift and Plumb 2008, Mielke et al. 2013, Clift et al. 2014) and in the interplay of glacial and interglacial epochs (Braconnot et al. 2012, Ruddiman 2014). The TP represents a dominant driver of climate variability all around the globe (Molnar et al. 2005). In particular, the thermodynamic and mechanical effect of the TP on the strength, spatial extent and seasonal evolution of the South and East Asian monsoon systems makes it an outstanding factor for low-frequency climate variations (Molnar and Rajagopalan 2012, Park et al. 2012, Tang et al. 2013a). The TP is also a key region of investigation for the current debate on anthropogenic climate change. Climate reconstructions and meteorological data attest tremendous warming rates and record high temperatures during recent decades to the TP region (Guo and Wang 2012, Guangliang et al. 2013) and climate model projections identify one of the hot spots of future climate change in the mountainous areas of Central Asia (Yang et al. 2012, IPCC 2013, Mannig et al. 2013).

The assessment of the anthropogenic interference with climate and its relevance for ecosystems and society requires that the magnitude of natural climate variations and their underlying mechanisms are well understood (e.g. Ruddiman 2014). Given this, this study is dedicated to several outstanding paleo-climatic episodes that we compare in a consistent modeling framework. A number of sensitivity studies with a high-resolution regional climate model (RCM) are presented to simulate climate equilibrium states: (1) during different stages of surface uplift of the TP, (2) during the last glacial

Climate
of the Past
Discussions

100   maximum (LGM), and (3) during the mid-Holocene (MH) climate optimum. These

101   episodes have been identified as major time slices of paleo-climatic variability

102   worldwide and in the TP region, in particular (e.g. Braconnot et al. 2012, Mielke et al.

103   2013, Clift et al. 2014, Ruddiman 2014).

104   In this study, we complement previous work with a focus on three objectives. The first

105   objective of our study addresses the former hypothesis from Prell and Kutzbach (1992),

106   suggesting that glacial versus interglacial boundary conditions during the Quaternary

107   can produce climate anomalies across the TP that are in the same order of magnitude

108   as during Cenozoic (last ~55 Ma) surface uplift. For this purpose, we compare these

109   different episodes for the first time by means of state-of-the-art climate models using a

110   coherent experimental design.

111   The second objective pertains to the generation of high-resolution patterns of paleo-

112   climate for the TP and surrounding regions. Typically, paleo-climatic episodes are

113   derived from the interpretation of proxy-data based on tree rings, sedimentary archives,

114   and stable isotope methods (Bartlein et al. 2011, Grießinger et al. 2011, Bershaw et al.

115   2012, Mischke et al. 2013, Saraswat et al. 2013). Here, we produce simulated climate

116   equilibrium states, prescribing the specific boundary conditions for the various paleo-

117   climatic episodes, which serve as a theoretical basis and benchmark for the

118   interpretation of proxy-data. In addition, some episodes during the early uplift period

119   are addressed where proxy-data are rarely available (Clift and Plumb 2008).

120   Our third objective aims at improving the spatiotemporal representation of paleo-

121   climate across Asia and the TP by relying on a high-resolution RCM.

122

123

124

Climate
of the Past
Discussions

2   Background and previous related work

The effect of the TP uplift on local and regional climate, with particular focus on the
Indian summer monsoon, was investigated in earlier work (Hahn and Manabe 1975),
revealing the general relationship between uplift and cooling and drying on the TP as
well as a strengthening of the South and East Asian monsoons (cf. Kutzbach et al.
1989, 1993). Since then, these basic mechanisms and climate responses have been
corroborated by a number of modeling studies with global models using increasing
resolution and complexity (e.g. Kitoh et al. 2010, Molnar and Rajagopalan 2012, Park
et al. 2012, Wu et al. 2012, Botsyun et al. 2016). Recently, Ma et al. (2014) have
demonstrated that the elevation of the Himalaya is more relevant to the changing
climate patterns in the Asian monsoon regions than the height of the TP itself. Zhang
et al. (2014) have prescribed several regionally differentiated uplift scenarios and draw
a rather heterogeneous picture of the climate response to surface uplift. Common to
these studies is that they are based on coarse-grid climate models which, probably,
cannot account for the finer-scale characteristics of lower atmospheric circulation,
precipitation and height-dependent temperature (Braconnot et al. 2012). The deficits
of state-of-the-art global climate models for the assessment of present-day climate on
the TP have been highlighted by Su et al. (2013). Harrison et al. (2014) have compared
paleo-climatological simulations from various climate models with available proxy-data
and pointed to a number of substantial biases over Asia. Kitoh et al. (2010) reported
some added value when they enhanced the model horizontal resolution of their uplift
experiments to 120 km. Finally, work by Botsyun et al. (2016) applied an isotope
tracking global general circulation model (LMDZ-iso) to investigate the effect of surface
uplift on precipitation $\delta^{18}O$. They document significant change in the isotopic

150   composition of precipitation during surface uplift, and estimate only ~40% of existing

151   stable isotope based plaleoaltimetry sample locations contain a signal of the plateau

152   surface uplift history. The work of Botsyun et al. (2016) highlights the importance of

153   paleoclimate studies for understanding the tectonic, surface uplift, history of large

154   orogenic plateaus.

155   As a consequence, RCMs have also been applied to paleo-climatological issues in the

156   TP and Asian monsoon regions. Zheng et al. (2004) have addressed the MH period at

157   a rather low resolution of 120 km. The LGM and MH have been compared by Ju et al.

158   (2007) who revealed an added value of their RCM at 60 km resolution with respect to

159   the driving global model. A similar result was obtained by Polanski et al. (2012) at 50

160   km resolution for the MH episode. Liu et al. (2008a,b) have used an RCM with a lower

161   resolution of 90 km but accounted for large number of individual and combined forcings,

162   indicating that changing vegetation, sea level and large-scale atmospheric circulation

163   play a more important role in glacial climate than greenhouse gas concentrations and

164   orbital parameters. In terms of the surface uplift process, Song et al. (2009) have

165   carried out a sequence of experiments with stepwise elevation increase but restricted

166   their simulation period to several months only. More recent RCM simulations with low

167   resolution but spatially differentiated uplift scenarios highlighted the crucial importance

168   of the Himalayan barrier effect for the Indian monsoon and the predominating impact

169   of the TP elevation on the East Asian monsoon system (Tang et al. 2013a), whereas

170   interannual monsoon variability is hardly affected by the uplift stages (Tang et al.

171   2013b).

172   In order to meet our main objectives, we pursue a dynamical downscaling approach

173   nesting the RCM REMO at 0.5° (~55 km) resolution into the global climate model

174   ECHAM5 (Li et al. 2016a,b; Mutz et al., 2016). For all paleo-climatic episodes the same

175 model setup is used in terms of domain, resolution, model physics and driving model,

176 albeit with different boundary conditions for surface uplift magnitude, LGM and MH

177 (see section 2). This approach allows for direct comparison of the resulting climate

178 anomalies with each other. Sensitivity studies over 12 to 40 years are realized which

179 ensures climate equilibrium states of sufficient length for a thorough statistical (cluster)

180 analyses. REMO has been successfully applied and evaluated for climatological issues

181 in Europe (Jacob et al. 2001), Africa (Paeth et al. 2005, 2009), South East Asia (Saeed

182 et al. 2011) and Central Asia (Mannig et al. 2013). In the paleo-climatological context,

183 it has been used in a former version with stable isotopes for uplift scenarios in the

184 Andean region (Insel et al. 2012). Paxian et al. (2016) have recently identified an added

185 value of REMO and other RCMs when it comes to decadal predictability in the West

186 African monsoon system. In the present study, REMO is applied for the first time to a

187 paleo-climatological problem in Asia, assuming that it represents a valuable and

188 efficient tool to generate high-resolution patterns of paleo-climatic episodes to be

189 compared with proxy- data.

190 The subsequent section is dedicated to the description of the model, the experimental

191 design, the validation data and the statistical methods. The results of our analysis are

192 presented in section 4 and discussed in section 5. The last section comprises the main

193 conclusions and a brief outlook.

194

195 **3 Modeling design, data and methods**

196

197 The dynamical downscaling is undertaken with the hydrostatic RCM REMO (Jacob

198 2001). It is nested in the atmospheric global climate model ECHAM5 as atmospheric

199 part of the Max-Planck Institute for Meteorology coupled general circulation model

Climate
of the Past

Discussions

200   ECHAM5/MPI-OM (Jungclaus et al. 2006). For all paleo-climatic episodes REMO is

201   run over the same model domain, extending from 50°E to 130°E and from the equator

202   to 60°N (see Fig. 1). In addition, the same horizontal and vertical resolution is used,

203   amounting to 0.5° and 27 levels, respectively. The current REMO version is based on

204   the improved land surface scheme from Hagemann and Dümenil (2003) and has been

205   successfully employed in various regions of the globe (e.g. Paeth et al. 2009, Saeed

206   et al. 2011, Insel et al. 2012, Mannig et al. 2013). The REMO setup used here has

207   been extensively evaluated by means of a number of sensitivity studies. Basically two

208   types of experiments have been performed which are described below.

209   The first type of REMO experiments addresses the uplift process of the TP. For this

210   purpose, the RCM in 0.5° resolution is nested into AMIP-type global simulations with

211   ECHAM5 using a horizontal spectral resolution of T63 (~1.875°), 19 vertical levels and

212   observed sea surface temperature and sea ice data from GISST (Rayner et al. 1996).

213   The uplift is accounted for by a stepwise approach, setting the model topography in

214   ECHAM5 and REMO to 100%, 75%, 50%, 25% and 0% of the present-day elevation.

215   According to current geological knowledge (e.g. Molnar et al. 2005, Mielke et al. 2013,

216   Clift et al. 2014), the topography is modified in the domain indicated by the red line in

217   the top panel of Fig. 2, comprising the TP itself, the Himalaya, the Pamir, the Hindukush,

218   the Tian Shan and the Southeast Asian highlands. In contrast, the Altai region in the

219   northern part of our model domain was built prior to the TP uplift and, hence, is not

220   modified (cf. Wang et al. 2006). In order to avoid an artificial trough in Central Asia, a

221   minimum height of 500 m above sea level is prescribed when reduced topography falls

222   below this threshold. This is in agreement with Le Pichon et al. (1992) who suggested

223   a base height of at least 500 m for the TP area prior to plateau uplift in the Cenozoic.

224   Along the borders of the region with modified elevation, the discontinuous transition

9

Climate
of the Past
Discussions

225   between modified and unmodified topography is smoothed by interpolation. The

226   resulting model topographies for the control run (100% elevation) and the 4 sensitivity

227   studies with stepwise reduction of elevation are displayed in Fig. 2. It is obvious that

228   for each simulation a continuous land surface without unnatural cracks and slopes is

229   given. In addition, a part of the present-day relative topography across the TP region

230   is retained. Note that we use a rather idealized uplift scenario without regionally

231   differentiated uplift rates (cf. Tapponnier et al. 2001, Tang et al. 2013a, Zhang et al.

232   2014) nor a modification of the land-sea mask (cf. Fluteau et al. 1999) in order to

233   facilitate the physical interpretation of the climate response to the stepwise uplift

234   process. The control run with present-day elevation covers the period 1961-2000, the

235   other time slices are also based on 40-year model periods. For validation and statistical

236   analysis the first 10 model years are skipped in order to remove some slight spin-up

237   effects during the first model years, as found in temperature and moisture of the

238   deepest soil layer.

239   The second type of REMO experiments pertains to the LGM and MH episodes. In this

240   case, REMO is nested in a higher-resolution ECHAM5 version with T106 (~1.125°)

241   and 31 vertical levels (Werner et al. 2011). This ECHAM5 version includes stable

242   isotopes and has been analyzed in terms of $\delta^{18}O$ trajectories (Li et al. 2016a,b) and

243   governing factors of $\delta^{18}O$ (Mutz et al. 2016). The boundary conditions for the LGM

244   and MH periods have been prescribed equally in ECHAM5 and REMO. This includes

245   greenhouse gas concentrations, land surface characteristics, land-sea mask due to

246   sea level changes (in ECHAM5), and orbital parameters (cf. Ruddiman 2014). The

247   specific boundary conditions for LGM and MH are described in detail by Dietrich et al.

248   (2013). They are in agreement with the guidelines of the Paleoclimate Modelling

249   Intercomparison Project Phase 3 (PMIP3, Arnold et al. 2009). Oceanic boundary

250 conditions and sea ice coverage for present-day, LGM and MH are taken from a

251 coupled ECHO-G model experiment (Lorenz and Lohmann 2004). In REMO, the

252 modified land cover classes are translated into monthly varying seasonal cycles of

253 background surface albedo, fractional vegetation cover and leaf area index in order to

254 account for the seasonal evolution of the Asian monsoon systems in a more

255 appropriate way. Given the modified ECHAM5 resolution and model settings in

256 ECHAM5 and REMO, an additional control run is realized covering the period 1978-

257 1989. 12-year model periods are also applied to the LGM and MH episodes, retaining

258 the last 10 years for model validation and statistical analysis of climate anomalies.

259 For the validation of the present-day climate simulated by ECHAM5 and REMO, we

260 rely on monthly temperature and precipitation data from the CRU data set, a gridded

261 data product based on station observations over land (Mitchell and Jones 2005), from

262 the NCEP (Kalnay et al. 1996) and ERA40 (Uppala et al. 2005) reanalyses, and from

263 the High Asia Reanalysis (HAR), a regional reanalysis with the RCM WRF at a

264 resolution of 0.3° covering the period 2000-2012 (Maussion et al. 2014) which

265 represents a benchmark for state-of-the-art high-resolution data sets for the TP region.

266 Satellite-based precipitation products such as TRMM have not been considered due

267 to distinct biases over the Himalaya and TP (cf. Barthi and Singh 2015). The LGM and

268 MH paleo-climatic episodes are compared with quantitative reconstructions of

269 temperature and precipitation from pollen-based proxy-data available over several 2°

270 x 2° grid boxes across the TP and eastern Asia (Bartlein et al. 2011). This data set is

271 also used as a reference for PMIP3 paleo-simulations.

272 The statistical significance of climate changes due to the uplift process and to the LGM

273 and MH boundary conditions, respectively, is assessed by means of a one-way

274 analysis of variance (Wilks 2006), taking the offset of the means due to the changing

Climate
of the Past

Discussions

Open Access

EGU

275 boundary conditions as treatment effect and the year-to-year changes within the

276 simulated time series as internal variability.

277 A special focus of our study is on the TP region and on the question whether climate

278 types have noticeably changed due to the various forcings. Therefore, a classification

279 of the Tibetan climate is carried out by a hierarchical cluster analysis combined with a

280 subsequent non-hierarchical k-means correction approach, dedicated to achieve

281 homogeneous clusters which are sharply distinguishable from each other (cf. Paeth et

282 al. 2005, Wilks 2006, Geng et al. 2014, Netzel and Stepinski 2016). The cluster

283 analysis is applied to the domain indicated by the rectangle in Fig. 1. It is based on

284 seven atmospheric variables, including annual-mean 2 meter temperature, annual

285 precipitation amount, annual temperature range, 10 meter zonal and meridional wind

286 components in January and July. Eight clusters have been found to provide the best

287 result in terms of interpretable and discriminable climate types across the TP and

288 surrounding regions.

289

290 **4 Results**

291

292 **4.1 Model validation**

293 A comparison of annual temperature and precipitation averaged over the cluster

294 domain (see Fig. 1) between REMO, ECHAM5 and various observational data sets is

295 depicted in Fig. 3. The validation period is 1978-1989. The respective control run from

296 REMO marks the origin of the graph and all other data sets are indicated as anomalies

297 with respect to this control run. Obviously, the considered gridded data and reanalyses

298 differ substantially. Especially, CRU is much drier in the TP region and NCEP

299 noticeably cooler than ERA40 and HAR. The uncertainty on behalf of the observational

300   data is at least as pronounced as the potential bias of the RCM REMO. In fact, REMO

301   is quite close to the ERA40 reanalysis and the HAR data set. Note that the latter

302   certainly represents a benchmark for present-day climate on the TP, but the available

303   data period 2000-2012 is rather short and does not coincide with the simulation periods

304   of ECHAM5 and REMO. The driving global climate model ECHAM5 is characterized

305   by a strong wet bias on the TP. This bias is considerably reduced by dynamical

306   downscaling and points to a clear added value of REMO compared with ECHAM5.

307   This is in line with the study by Mannig et al. (2013) who have validated REMO

308   simulations driven by ERA40 reanalyses and ECHAM5/MPI-OM coupled climate

309   model simulations over entire Asia and concluded that the RCM performs well over the

310   continent and exhibits an added value with respect to the coarser-grid global climate

311   model.

312   A more detailed validation of REMO in the model domain and version presented here

313   has been conducted in the framework of a PhD project (unpublished PhD thesis in

314   2015 by Christian Steger). It has been demonstrated that REMO is able to reproduce

315   the observed main characteristics of climate on the TP and in surrounding regions.

316   Especially temperature at high-elevation sites is well captured and clusters of distinct

317   climate types agree almost perfectly between REMO, ERA40 and HAR. Therefore, it

318   is assumed that REMO provides a reliable basis to simulate paleo-climatic changes.

319

320   **4.2 Surface uplift experiments**

321   The temperature changes associated with the surface uplift of the TP and surrounding

322   mountain areas are illustrated in Fig. 4. As the plateau itself and the Asian monsoon

323   systems are subject to a distinct seasonal regime, results are shown for annual means,

324   winter means (DJF) and summer means (JJA). Indeed, the annual temperature range

325   increases from south to north and amounts to more than 40°C between winter and

326   summer in Central Asia and in parts of the TP (Fig. 4, top panels). It is also obvious

327   that near-surface temperature is a stringent function of elevation. Thus, reduced

328   elevation leads to higher temperature over the TP, simply due to the thermal

329   stratification of the atmosphere (Fig. 4, panels d-o). The warming amounts to more

330   than 10°C in the experiment with 0% of present-day elevation (with a minimum height

331   of 500 m on the TP). Interestingly, it is a nonlinear function of reduced topography

332   since the warming exhibits larger magnitudes in the 75% and 50% experiments than

333   in the 25% and 0% experiments. On the TP itself, warming rates in winter and summer

334   are virtually the same. Central Asia is marked by a slight cooling and the continental

335   desert region north of the TP by a noticeable cooling in both seasons, amounting to

336   more than 7°C, especially in winter. Later on, this will be explained by precipitation and

337   circulation changes. Over South Asia, reduced elevation implies lower temperature in

338   winter and slightly warmer conditions in summer. While the first effect is associated

339   with enhanced cold air advection from the continent due to the missing barrier of the

340   Himalaya and TP, the latter effect is linked to reduced precipitation amount (see below).

341   Thanks to the high resolution of REMO, the resulting climate change patterns are

342   characterized by numerous regional details such as the basin structure on the

343   northeastern TP, the fine-scale changes in the Tian Shan mountain range and the

344   desert basins in western China.

345   The impact of the stepwise uplift on annual, winter and summer precipitation is

346   portrayed in Fig. 5. In the South and East Asian monsoon regions precipitation is

347   mainly a summer phenomenon, whereas the mid-latitudes in Asia follow a more

348   equalized seasonal regime (Fig. 5, top panels). The precipitation response to reduced

349   elevation is marked by a spatially heterogeneous picture (Fig, 5, panels d-o). The TP,

Climate
of the Past
Discussions

EGU

350   South Asia, eastern China and the southern part of Central Asia exhibit drier conditions.

351   In the monsoon areas this amounts to less than 50%. In Central Asia the relative drying

352   is more important. However, the most striking feature in the precipitation response is

353   simulated over the continental arid regions of western China and northwestern Central

354   Asia. Indeed, precipitation increases by up to 250%, when the plateau height is

355   reduced to 25%. This rises to up to four times more than the present-day climatology

356   in some arid regions and is related to circulation changes (see below). Again, the major

357   changes occur up to a reduction to 25% of present-day elevation, while the 0%

358   experiment only increases the precipitation signal on the TP itself. An interesting

359   regional detail is given by the wetter conditions in winter along southeastern India and

360   Southeast Asia, where the missing barrier effect of the Himalaya and TP leads to more

361   relief rainfall from the continental winter monsoon flow.

362   To assess the importance and statistical significance of temperature and precipitation

363   changes due to the uplift process, a one-way analysis of variance has been applied

364   using pairs of uplift experiments or all uplift experiments at once. The analysis of

365   variance reveals that the stepwise uplift scenario accounts for more than 90% of total

366   annual temperature variability on the TP (Fig. 6, top panels). This implies that the

367   topographic forcing between the 30-year time slices dominates by far the internal year-

368   to-year fluctuations of temperature within the time slices. This effect is already

369   achieved in the 75% experiment. In the surrounding regions, the uplift effect is less

370   pronounced, ranging between 20% and 80% of explained variance. Nevertheless, the

371   temperature changes are statistically significant in almost the entire model domain. For

372   precipitation the picture is more dispersed and the uplift effect is much less pronounced

373   in the 75% experiment: Precipitation is characterized by substantially stronger internal

374   variability than temperature (e.g. IPCC 2013) and, hence, the uplift process accounts

15

Climate
of the Past
Discussions

375   for a smaller portion of total variance. Nonetheless, the explained variance reaches up

376   to 90% in the arid regions of western China, where the uplift comes along with a

377   multiplication of present-day precipitation amount.

378   In the following, the substantial drying of the desert basins of western and northern

379   China during the uplift phase is analyzed in more detail. At first sight, this may be

380   interpreted as an increasing barrier effect of the topography, hindering the moist

381   summer monsoon flow from the northern Indian Ocean to penetrate far into the Asian

382   continent. However, a deeper look on the wind components in various atmospheric

383   levels before and after the uplift reveals that in none of the uplift experiments the

384   monsoon air masses propagate into the arid regions of western China, rather these

385   are characterized by extratropical westerlies independent of the topography (not

386   shown). The clue to the problem is given by changes in the extratropical wave train.

387   Fig. 7 displays the mean position of troughs and ridges in the 500 hPa geopotential

388   height field under present-day conditions (top panel) and the respective changes in the

389   50% and 0% experiments (bottom panels). Currently, long-term mean geopotential

390   height is higher over Central Asia and lower over northeastern Asia, indicating the

391   typical position of ridges and troughs, respectively, in the extratropical Rossby waves.

392   Apparently, reduced elevation of the TP implies a substantial large-scale decrease of

393   geopotential height over Central Asia, leading to more advection of moist air masses

394   at the forefront of the trough which is located exactly over the region where the

395   precipitation increase peaks in northwestern China. This appears to be the key

396   mechanism of how the uplift process in the TP regions affects extratropical climate all

397   around the globe (cf. Molnar et al. 2005).

398   The last aspect addressed from the uplift experiments pertains to the identification of

399   distinct climate types on the TP and adjacent regions and their sensitivity to the uplift

Climate
of the Past
Discussions

400   process. In the high-dimensional climate system, climate types often allow for a more

401   comprehensive interpretation of climate changes than individual grid boxes (e.g. Paeth

402   et al. 2005, Geng et al. 2014, Netzel and Stepinski 2016). Fig. 8 presents a climate

403   classification based on eight clusters derived from the 30-year REMO control run (top

404   panel). The clusters are arranged from warm climates (red) to cold climates (blue). The

405   remaining panels refer to the experiments with reduced elevation, but use the cluster

406   centroids from the control run. Under present-day conditions, the desert Tharr in

407   western India occupies cluster 1 which is characterized by very high temperature and

408   low annual rainfall amount. Northwestern India is marked by cluster 2 with still rather

409   high temperature but more humid conditions. Cluster 3 represents the southern slopes

410   of the Himalaya where climate is cooler but annual precipitation exceeds 3000 mm/yr.

411   Cluster 4 is characterized by intermediate temperature and very dry conditions and

412   covers the continental deserts with less than 100 mm of annual precipitation,

413   particularly in the Tarim basin. Cluster 5 extends along the foothills on the northern

414   side of the TP, the Tian Shan and the Pamir as well as over the less arid regions of

415   western China. It denotes a colder and more humid climate than cluster 4. The

416   southern and eastern part of the TP is given by cluster 6. Annual mean temperature is

417   below 0°C and rainfall exceeds 1500 mm per year. This cluster denotes those parts of

418   the TP on the wind-ward side that are more influenced by moist air advection from the

419   South Asian summer monsoon. In contrast, cluster 8 stands for the much drier and

420   even colder northern part of the TP. Cluster 7 is rather peculiar: it spreads over those

421   areas of the plateau that are marked by a large number of lakes. In the vicinity of these

422   lakes, REMO simulates a climate that is as cold as the one in cluster 8 but with

423   precipitation totals of up to 2000 mm/year. Later on, this cluster will be identified as a

424   model artefact.

425   The experiments with reduced topography manifest a stepwise shift of these climate

426   types towards a setting where the TP exhibits a much warmer and drier climate. North

427   of the TP, climate switches from the continental desert type to a much colder and more

428   humid type which is confined today to the lee side of the TP. Altogether, the climate

429   classification of the 0% experiment leads to a pattern which fundamentally differs from

430   the one under present-day conditions, highlighting the tremendous impact of the uplift

431   process on climate types on and around the TP. It is also intriguing that the shift of the

432   clusters mainly takes place when the elevation is reduced to 25% and 0% of the current

433   topography.

434

435   4.3 Mid-Holocene and LGM experiments

436   The simulated temperature anomalies during the LGM and MH episodes are illustrated

437   in Fig. 9. Again, it is differentiated between annual, winter and summer means. Note

438   that the control run for these time slices is slightly different from the one for the uplift

439   experiment and only 10 years per run are available for analysis because the ECHAM5

440   simulations used for the lateral boundary conditions have much higher resolution and,

441   thus, have been computationally more expensive. It is obvious that the temperature

442   response during the LGM period is much more pronounced than during the MH time

443   slice. The LGM exhibits lower temperatures in virtually the entire model domain. The

444   cooling amounts to 3-8°C with largest amplitude on the TP.

445   During the MH, the picture is more heterogeneous and temperature changes do not

446   exceed 3°C. Most regions undergo slightly colder conditions, except for the

447   extratropical part of Asia in summer. Again, the cooling effect peaks over the TP and,

448   in particular, along the southern foothills of the Himalaya.

Climate
of the Past
Discussions

449 The precipitation response during the LGM and MH periods is spatially rather

450 incoherent (Fig. 10). During the LGM, drier conditions prevail in most parts of Asia,

451 especially in Central Asia and the Middle East. Higher-elevation sites with southward

452 exposition along the Himalaya, the Pamir, the Tian Shan and the Altai may have

453 experienced more precipitation. The most striking feature, however, is the enormous

454 rainfall increase in winter by more than 100% over eastern India, Bangladesh and parts

455 of Southeast Asia. This increase during the northeasterly winter monsoon flow is

456 contradictory to the present-day seasonality. We have no reasonable physical

457 explanation for such a process and assume it to be a model artefact, possibly arising

458 from a misrepresentation of the prescribed oceanic boundary conditions in the Bay of

459 Bengal that produces a prominent wet bias inland (cf. Paeth et al. 2005).

460 The MH episode appears to be subject to slightly more annual precipitation amount in

461 most parts of the model domain, except for Central India and the Middle East. This

462 increase mainly takes place during the summer season, initiated by a stronger

463 monsoon flow in East Asia and more advection of moist air masses by westerlies in

464 the extratropics. The pattern of summer precipitation changes is consistent with the

465 temperature response in Fig. 9: higher temperatures north of the TP provoke a

466 northward shift of the summer monsoon flow with more rainfall along the Himalaya and

467 the TP. Vice versa, higher rainfall in northern India and over the foothills of the

468 Himalaya implies a cooling in these areas.

469 The analysis of variance demonstrates that the impact of LGM and MH boundary

470 conditions on temperature and precipitation does not everywhere stand out from

471 internal variability (Fig. 11). During the LGM period, the effect on near-surface

472 temperature is outstanding with more than 90% of explained variance, especially on

473 the TP, in Central Asia and the Middle East. In contrast, the MH episode comes along

19

Climate
of the Past
Discussions

Open Access

EGU

474   with a weaker temperature response, which peaks over South and Southeastern Asia.

475   Only a part of the TP region is significantly affected by the MH boundary conditions.

476   Typically, the forcing accounts for 20% to 70% of total temperature variance. For

477   precipitation, the picture is more dispersed: the MH is barely characterized by a

478   coherent rainfall response pattern and, thus, the changes denoted in Fig. 10 should

479   not be over-interpreted, except for the wetter conditions in the southern and western

480   part of the TP. The LGM only leaves a mark in western and southeastern Asia where

481   precipitation is below present-day totals. However, the explained variance ranges

482   mostly below 50%.

483   In Fig. 12 the simulated annual temperature and precipitation changes during the LGM

484   and MH episodes are compared with available quantitative reconstructions from

485   pollen-based proxy-data (Bartlein et al. 2011). Note that in contrast to Fig. 10 the

486   precipitation response is expressed in mm per year and not in percentage. The MH

487   period is much better represented by proxy-data than the LGM (cf. Clift and Plumb

488   2008, Bartlein et al. 2011). During the LGM episode, there is a good agreement

489   between simulated and reconstructed temperature and precipitation, although this

490   comparison is based on a small number of grid boxes. Colder and drier conditions over

491   China and Central Asia are likewise suggested by REMO and proxy-data. The two

492   neighboring reconstructed pixels over the western Tian Shan with opposite

493   temperature changes obviously reflect a data artefact. Unfortunately, the simulated

494   phenomenon of substantial rainfall increase north of the Bay of Bengal (see Fig, 10)

495   can neither be confirmed nor falsified by proxy-data by reason that they are not

496   available in this region.

497   During the MH, the pattern is more complex: reconstructions indicate a small-scale

498   coexistence of warmer and colder conditions over the TP, China and Central Asia,

Climate
of the Past
Discussions

499   whereas in REMO a slight cooling prevails over most of the model domain. On the part

500   of the reconstructions, the temperature response varies by up to 10°C, partly with

501   opposite sign, over a distance of some hundreds of kilometers. This reflects a large

502   amount of uncertainty in the proxy-data, while the RCM produces a spatially coherent

503   response pattern. In terms of precipitation, there is a satisfactory agreement between

504   model and reconstructions: wetter conditions prevail over the TP, China and parts of

505   Central Asia.

506   Finally, Fig. 13 clearly reveals that the spatial distribution of main climate types over

507   the TP and surrounding regions is more or less insensitive to the modified boundary

508   conditions during the LGM and MH periods. Note that in this case the reference

509   clusters for present-day climate have been derived from a shorter period and, hence,

510   the pattern differs slightly from the one in Fig. 8. Under LGM and MH conditions the

511   climate classification barely changes. This is somewhat contradictory to the simulated

512   temperature and precipitation changes presented in Figs. 9 and 10, especially with

513   respect to the considerably colder conditions during the LGM. The fact that the clusters

514   still remain stationary is a clear indication that the other atmospheric variables entering

515   the cluster analysis – i.e. wind components, annual temperature range and, to a certain

516   extent, precipitation – are hardly affected by the modified boundary conditions during

517   LGM and MH. This is a major difference from the uplift experiments (see Fig. 8).

518

519   **4.4   Comparison of episodes**

520   In the last step of our analysis the annual temperature and precipitation changes under

521   uplift, LGM and MH conditions are directly compared with each other, once as regional

522   means over the entire cluster domain and once as averages over each individual

523   cluster (Fig. 14). In addition, the results from REMO and ECHAM5 are compared with

Climate
of the Past

Open Access

Discussions

EGU

524   each other in order to assess which model type is associated with a higher sensitivity.

525   Over the cluster domain, the strongest temperature and precipitation response is found

526   for the uplift experiments, denoting a noticeably drier and warmer climate on and

527   around the TP (top left panel). There is an offset between ECHAM5 and REMO (cf.

528   Fig., 3) but the response is very similar. In both models, the largest changes occur

529   between the 100%, 75% and 50% experiments, whereas the uplift from 0% to the 25%

530   simulation plays a minor role. The LGM and MH affect the mean climate in the cluster

531   domain to a much lower extent. The response in REMO and ECHAM5 is again similar,

532   with one exception: REMO simulates slightly wetter conditions, mainly due to the

533   outstanding precipitation increase over the southeastern TP (see Fig. 10), while

534   ECHAM5 suggests a drying.

535   Fig. 14 also indicates that the striking climate changes during the uplift process are

536   mainly performed by clusters 3, 6, 7 and 8. These clusters represent the higher-

537   elevation sites and southward slopes of the TP and Himalaya. The changes in cluster

538   3 and 8 even lie outside the illustrated precipitation and temperature range,

539   respectively, highlighting the enormous drying along the southern slope and warming

540   on the northern TP at reduced elevation. In addition, clusters 4 and 5 experience a

541   substantial precipitation increase in the 25% and 0% experiments, suggesting that the

542   continental dry climate north of the TP has not yet existed during the early uplift phase

543   (cf. Fig. 5). This effect is only simulated by REMO at higher spatial resolution. LGM

544   and MH have mainly affected the clusters 3, 4, 5 and 6. Clusters 4 and 5 are

545   representative of the arid and semi-arid climate types north of the TP. Nonetheless,

546   temperature over the TP (clusters 7 and 8) also decreases considerably under LGM

547   conditions. In most cluster regions around the TP, the climate changes during LGM

548   and MH range are of the same order of magnitude as during the uplift process. In

Climate
of the Past
Discussions

549   contrast, the TP itself is much more sensitive to the plateau uplift and, hence, stronger

550   signals should be expected in proxy-data for that earlier period.

551

552   **5   Discussion**

553

554   This study provides new insight into prominent Cenozoic and Quaternary paleo-

555   climatic variations in Asia and, more specifically, in the TP region. The comparative

556   validation of the RCM REMO and the driving global climate model ECHAM5 has shown

557   that the higher-resolution model is closer to the available observational data and

558   reanalyses, particularly with respect to precipitation. This is consistent with other

559   studies highlighting the added value of higher-resolution climate models in Asia and

560   other regions of the globe (e.g. Kitoh et al. 2010, Paeth et al. 2011, Mannig et al. 2013,

561   Paxian et al. 2016).

562   The uplift experiments with stepwise reduction of topography describe a continuous

563   transition towards a warmer and drier climate on the TP when elevation decreases.

564   This general tendency has been found in virtually all uplift experiments since the

565   pioneering work by Hahn and Manabe (1975) and Kutzbach et al. (1989, 1993).

566   Another earlier finding, which we could corroborate with this study, is the fact that the

567   later uplift process has played a more important role for the TP climate and surrounding

568   monsoon systems than the early phase. In our study, the changes are stronger

569   between the 100%, 75% and 50% experiments than between the 25% and 0%

570   simulations. Kitoh et al. (2010) have reported that their 60% experiment represented a

571   threshold for accelerated climate change. A novel aspect of our modeling design

572   pertains to the high spatial resolution and, at the same time, the relatively long

573   simulation periods for the time slices, which allow for a more sophisticated statistical

Climate
of the Past
Discussions

574   assessment of changes and their significance. A new finding arising from the high

575   resolution of the REMO model concerns the appearance of the continental-desert type

576   of climate that first occurred in the transition from the 25% to the 50% experiment. This

577   process is probably related to dynamical changes in the extratropical Rossby wave

578   configuration. The identification of climate types by means of cluster analysis has

579   proven to be an instructive tool to illustrate changes at the scale of regional climates

580   (cf. Geng et al. 2014, Netzel and Stepinski 2016). In fact, it could be shown that the

581   uplift process induces a fundamental rearrangement of present-day climate types on

582   the TP and in surrounding regions, especially to the north.

583   During the LGM period, REMO simulates colder conditions in most regions of Asia with

584   the largest temperature decrease in winter over the TP and in the northernmost part of

585   the model domain along 60°N. This is in agreement with previous modeling studies

586   (e.g. Liu et al. 2008a,b, Harrison et al. 2014) and reconstructions (e.g. Mischke et al.

587   2013, Saraswat et al. 2013). The cooling in our model ranges between 3°C and 8°C

588   on the TP which agrees well with proxy-data from Bartlein et al. (2011). In contrast,

589   other authors have stated that the LGM cooling rate is underestimated by their global

590   (Harrison et al. 2014) and regional (Zheng et al. 2004, Ju et al. 2007) climate models.

591   In terms of precipitation, the pattern is dominated by drier conditions in most of the

592   model domain. However, precipitation amount over the TP itself is mainly unaffected,

593   except for an extensive increase in the southeastern part, which we assign to a model

594   artefact. In general, precipitation changes are strongly superimposed by internal

595   variability within the time slices. Despite the noticeable cooling tendency, the spatial

596   arrangement of climate types during the LGM episode can hardly be distinguished from

597   the present-day situation, mainly because atmospheric circulation is more or less

598   unchanged.

Climate
of the Past
Discussions

599   The temperature effect during the MH period is minor compared with the other paleo-

600   climatic time slices. A slight cooling of less than 1°C prevails over most of Asia. Over

601   the TP and northern India it reaches up to 3°C. During summer, the extratropical part

602   of the model domain experiences some warming by 1-2°C. While this minor cooling

603   tendency in REMO is consistent with the majority of temperature reconstructions in

604   central and eastern Asia (cf. Bartlein et al. 2011, Braconnot et al. 2012), it disagrees

605   with former modeling approaches for the MH period which suggest a slight warming

606   (Zheng et al. 2004, Polanski et al. 2012, Harrison et al. 2014). Concerning precipitation,

607   our model confirms the wetter conditions over the TP, northern India, eastern Asia and

608   northern China as suggested by other authors (e.g. Zheng et al. 2004, Polanski et al.

609   2012, Saraswat et al. 2013). Yet, the precipitation changes hardly stand out from the

610   internal variability within the MH time slice. The climate classification during the MH is

611   also largely congruent with the one under present-day conditions.

612   The application of a uniform downscaling approach with an RCM using the same model

613   domain, resolution and model physics allows for a direct comparison of climate change

614   signals among all considered time slices, which is unprecedented for uplift, LGM and

615   MH episodes. Not surprisingly, the uplift process is associated with the largest

616   temperature and precipitation response and shift of climate types, at least on the basis

617   of the entire TP region. These regional-mean changes hardly differ between REMO

618   and ECHAM5. In both models, the uplift mainly affects the high-elevation clusters over

619   the TP. However, the disappearance of the arid climate types north of the TP in the

620   25% and 0% experiments is a feature that only occurs at higher resolution in REMO.

621   Another interesting finding is that at the scale of individual clusters, i.e. regional

622   climates, glacial and, to a lower extent, MH conditions can provoke climate anomalies

623   in the same order of magnitude as the uplift process. This mainly pertains to the climate

Climate
of the Past
Discussions

624   types in northern India and along the southern slopes of the Himalaya. Thus, the former

625   hypothesis by Prell and Kutzbach (1992) can be supported by our model results.

626

627   **6   Conclusions**

628

629   The main objectives of the present study were to assess and compare paleo-climatic

630   changes in Asia and, especially, in the TP region. For this purpose, we have carried

631   out a series of RCM experiments that are characterized by high spatial resolution and

632   sufficiently long simulation periods to account for the impacts of uplift, LGM and MH

633   boundary conditions on the regional climate and to allow for a comparison with

634   available climate reconstructions from proxy-data. The modeling design was such that

635   a direct comparison of all considered paleo-climatic episodes is ensured.

636   Our first objective pertained to the former hypothesis by Prell and Kutzbach (1992),

637   suggesting that glacial boundary conditions can produce similar climate changes as

638   the uplift process during the Miocene-Pliocene period. This hypothesis could be

639   confirmed on the basis of regionally confined climate types, especially to the south of

640   the TP. However, at the scale of the entire region of the TP and adjacent areas, climate

641   is clearly more sensitive to the uplift than to Quaternary forcings during the LGM and

642   MH periods.

643   The second main objective referred to the generation of high-resolution patterns of

644   paleo-climatic states that are suitable for a quantitative comparison with climate

645   reconstructions. For the LGM period, this comparison is successful but based on a

646   very small number of grid boxes. The proxy-data for the MH episode are more

647   numerous and wide-spread over Asia. However, they exhibit substantial uncertainty,

648   drawing a picture of substantial temperature rise and decrease at neighboring locations.

Climate
of the Past
Discussions

649   In contrast, our model produces patterns of paleo-climatic anomalies that are spatially

650   more coherent and physically consistent. Therefore, we suggest that RCMs are able

651   to provide a valuable theoretical basis for the assessment of paleo-climate and the

652   climatological interpretation of proxy-data.

653   The third objective aimed at improving the spatiotemporal representation of paleo-

654   climatic episodes in Asia. Indeed, the simulation periods of 12 to 40 years per time

655   slice allowed for a sophisticated statistical analysis of climate changes in order to

656   distinguish between real climate change signals and climate anomalies that do not

657   stand out from internal variability. The horizontal resolution of 0.5° used in the RCM

658   REMO has proven to add value to the representation of climate across the TP,

659   compared with the driving global climate model. This relates to the model bias in terms

660   of present-day climate, the regional details of simulated climate patterns – especially

661   for the cluster analysis – and some new insights into climate changes north of the TP,

662   i.e. the appearance of the arid climate types in western China when the TP reaches at

663   least 50% of its present-day elevation.

664   There is still room for improvement of the model itself, the modified boundary

665   conditions and the number of experiments. First of all, the matrix of paleo-climatic

666   simulations could be extended, accounting for spatially differentiated uplift scenarios

667   (cf. Tapponnier et al. 2001, Tang et al. 2013a, Zhang et al. 2014), modified paleo-

668   geography (Fluteau et al. 1999), and a decomposition of forcings during the LGM and

669   MH periods (Liu et al. 2008a,b, Polanski et al. 2012). This would lead to a more

670   comprehensive understanding of the processes leading to paleo-climatic changes but,

671   at the same time, require enormous computing resources beyond the scope of our

672   project. In addition, simulations over several hundreds or thousands of years would

673   help to assess the superposition of time scales of climate fluctuations and changes

Climate
of the Past
Discussions

674   arising from internal and external sources of variability, respectively (cf. Lorenz and

675   Lohmann 2004).

676   The RCM REMO has been shown to have a good performance in terms of the

677   prominent features of regional climate in Asia and on the TP. Some systematic biases

678   can still be removed by statistical post-processing (e.g. Paeth 2011). However, a major

679   deficit is the simulation of precipitation over high-elevation lakes on the TP where

680   surface water temperature in winter is substantially overestimated and precipitation

681   amount by far too high. In the future, this problem will be tackled by implementing the

682   lake model FLake (Mironov et al. 2010) in REMO. Some further improvements can be

683   expected when REMO is used in a version that is fully coupled to an ocean model

684   enhancing the physical consistency of the climate simulations (cf. Sein et al. 2015).

685   Recently, Gao et al. (2015) have implemented a more realistic land cover classification

686   in REMO and reported an enhanced skill of the model. Finally, the aspect of model

687   uncertainty must be addressed also for the assessment of paleo-climatic changes, e.g.

688   by running a multi-model ensemble of RCMs nested into different global climate

689   models from the PMIP3 initiative. Combining this with the matrix of more sensitivity

690   studies implies an enormous computational effort that could be achieved in the

691   framework of a potential future paleo-CORDEX initiative.

692

693   **Acknowledgements**

694

Climate
of the Past
Discussions

Open Access

EGU

References

Arnold, L., F.-M. Bréon, and S. Brewer (2009), The Earth as an extrasolar planet: the vegetation spectral signature today and during the last Quaternary climatic extrema, Int. J. Astrobiol. 8, 81.

Barthi, V., and C. Singh (2015), Evaluation of error in TRMM 3B42V7 precipitation estimates over the Himalayan region, J. Geophys. Res. 120, 12458-12473.

Bartlein P.J. and 18 co-authors (2011), Pollen-based continental climate reconstructions at 6 and 21 ka: a global synthesis, Climate Dyn. 37, 775-802.

Bershaw, J., S.M. Penny, and C.N. Garzione (2012), Stable isotopes of modern water across the Himalaya and eastern Tibet: Implications for estimates of paleoelevation and paleoclimate, J. Geophys. Res. 117, doi:10.1029/2011JD016132.

Botysun, S., Sepulchre, P., Risi, C., and Y. Donnadieu (2016), Impacts of Tibetan Plateau uplift on atmospheric dynamics and associated precipitation δ^{18}O, Clim. Past. 12, doi:10.519/cp-12-1401-2016.

Braconnot, P., S.P. Harrison, M. Kageyama, P.J. Bartlein, V. Masson-Delmotte, A. Abe-Ouchi, B. Otto-Bliesner, and Y. Zhao (2012), Evaluation of climate models using Palaeoclimatic data, Nature Climate Change 2, 417-424.

Clift, P.D., and R.A. Plumb (2008), The Asian monsoon: causes, history and effects, Cambridge Univ. Press.

Clift, P.D., R. Tada, and H. Zheng (2014), Monsoon evolution and tectonics-climate linkage in Asia: an introduction, Geol. Soc. London, Special Publ. 342, 1-4.

Dietrich, S., M. Werner, T. Spangehl, and G. Lohmann (2013), Influence of orbital forcing and solar activity on water isotopes in precipitation during the mid- and llate Holocene, Clim. Past 9, 13-26.

Fluteau, F., G. Ramstein, and J. Besse (1999), Simulating the evolution of the Asian and African monsoons during the past 30 Myr using an atmospheric general circulation model, J. Geophys. Res. 104, 11995-12018.

Gao, Y., S. Weiher, T. Markkanen, J.-P. Pietikänen, H. Gregow, H.M. Henttonen, D. Jacob, and A. Laaksonen (2015), Implementation of the CORINE land use classification in the regional climate model REMO, Boreal Environ. Res. 20, 261-282.

Geng, Q., P. Wu, X. Zhao, and Y. Wang (2014), Comparison of classification methods for the division of wet/dry climate regions in Northwest China, Int. J. Climatol. 34, 2163-2174.

Grießinger, J., A. Bräuning, G. Helle, A. Thomas, and G. Schleser (2011), Quaternary Holocene Asian summer monsoon variability reflected by d18O in tree-ring from Tibetan junipers, Geophys. Res. Lett. 38, L03701.

Guangliang, H., E. Chongyi, and L. Xiangjun (2013), Reconstruction of integrated temperature series of the past 2000 years on the Tibetan Plateau with 10-year intervals, Theor. Appl. Climatol. 113, 259-269.

Guo, D., and H. Wang (2012), The significant climate warming in the northern Tibetan Plateau and its possible causes, Int. J. Climatol. 32, 1775-1781.

Hagemann S., and L. Dümenil Gates (2003), Improving a subgrid runoff parameterization scheme for climate models by the use of high resolution data derived from satellite observations, Climate Dyn. 21, 349--359.

Hahn, D.G., and S. Manabe (1975), The role of mountains in the South Asian monsoon circulation, J. Atmos. Sci. 32, 1515-1541.

751   Harrison, S.P., P.J. Bartlein, S. Brewer, I.C. Prentice, M. Boyd, I. Hessler, K. Holmgren,

752   K. Itzumi, and K. Willis (2014), Climate model benchmarking with glacial and mid-

753   Holocene climates, Clim. Dyn. 43, 671-688.

754   Insel, N., C.J. Poulsen, T.A. Ehlers, and C. Sturm (2012), Response of meteoric d18O

755   to surface uplift – Implications for Cenouoic Andean Plateau growth, Earth Planet.

756   Sci. Lett. 317-318, 262-272.

757   IPCC (2013), Climate Change 2013, The Physical Science Basis, Working Group I

758   Contribution to the Fifth Assessment Report of the Intergovernmental Panel on

759   Climate Change, Cambridge Univ. Press, Cambridge, 1535 pp.

760   Jacob D. (2001), A note to the simulation of the annual and interannual variability of

761   the water budget over the Baltic Sea drainage basin, Meteorol. Atmos. Phys. 77,

762   61--74.

763   Ju, L. H. Wang, and D. Jiang (2007), Simulation of the Last Glacial Maximum climate

764   over East Asia with a regional climate model nested in a general circulation model,

765   Palaeogeography, Palaeoclimatology, Palaeoecology 248, 376-390.

766   Jungclaus, J.H., N. Keenlyside, M. Botzet, H. Haak, J.J. Öuo, M. Latif, J. Marotzke, U.

767   Mikolajewicz, and E. Roeckner (2006), Ocean circulation and tropical variability in

768   the coupled model ECHAM5/MPI-OM, J. Climate 19, 3952-3972.

769   Kalnay E., M. Kanamitsu, R. Kistler, W. Collins, D. Deaven, L.S. Gandin, M. Iredell, S.

770   Saha, G. White, J. Woolen, Y. Zhu, M. Chelliah, W. Ebisuzaki, W. Higgins, J.

771   Janowiak, K.C. Mo, C. Ropelewsky, J. Wang, A. Leetma, R. Reynolds, R. Jenne

772   and D. Joseph (1996), The NCEP/NCAR 40-year Reanalysis Project, Bull Amer

773   Meteor Soc 77, 437–471.

774   Kitoh, A., T. Motoi, and O. Arakawa (2010), Climate modelling study on mountain uplift

775   and Asian monsoon evolution, Geol. Soc. London, Special Publ. 342, 293-301.

Climate
of the Past
Discussions

Open Access

EGU

776   Kutzbach, J.E., P.J. Guetter, W.F. Ruddiman, and W.L. Prell (1989), Sensitivity of

777   climate to Quaternary Cenozoic uplift in southern Asia and the American West:

778   Numerical experiments, J. Geophys. Res. 94, 18393-18407.

779   Kutzbach, J.E., W.L. Prell, and W.F. Ruddiman (1993), Sensitivity of Eurasian climate

780   to surface uplift of the Tibetan Plateau, J. Geology 101, 177-190.

781   Le Pichon, X., M. Fournier, and L. Jolivet (1992), Kinematics, topography, shortening,

782   and extrusion in the India-Eurasia collision, Tectonics 11, 1085-1098.

783   Li, J., T.A. Ehlers, S. Mutz, C. Steger, H. Paeth, M. Werner, C.J. Poulsen, R. Feng

784   (2016), Modern precipitation d18O and trajectory analysis over the Himalaya-Tibet

785   orogen from ECHAM5-wiso simulations, J. Geophys. Res., under revision.

786   Li, J., T.A. Ehlers, M. Werner, S. Mutz, C. Steger, and H. Paeth (2016), Quaternary

787   Quaternary climate, precipitation d18O, and Indian Monsoon variations over the

788   Tibetan Plateau, Earth Planet. Sci. Lett., under revision.

789   Liebke, U., E. Appel, L. Ding, and Q. Zhang (2013), Age constraints on the India-Asia

790   collision derived from secondary remanences of Tethyan Himalayan sediments from

791   the Tingri area, J. Asian Earth Sci. 62, 329-340.

792   Liu, Y., J. He, W. Li, and L. Chen (2008a), MM5 simulations of the China regional

793   climate during the LGM. I: Influence of CO2 and Earth orbit change, Acta Meteorol.

794   Sinica 22, 8-21.

795   Liu, Y., J. He, W. Li, and L. Chen (2008b), MM5 simulations of the China regional

796   climate during the LGM. I: Influence of change of land area, vegetation, and large-

797   scale circulation background, Acta Meteorol. Sinica 22, 22-30.

798   Lorenz, S., and G. Lohmann (2004), Acceleration technique for Milankowitch type

799   forcing in a coupled atmosphere-ocean circulation model: method and application

800   for the Holocene, Clim. Dyn. 23, 727-743.

801   Ma, D., W. Boos, and Z. Kuang (2014), Effects of orography and surface heat fluxes

802   on the South Asian summer monsoon, J. Climate 27, 6647-6659.

803   Mannig, B., M. Müller, E. Starke, C. Merkenschlager, W. Mao, X. Zhi, R. Podzun, D.

804   Jacob, and H. Paeth (2013), Dynamical downscaling of climate change in Central

805   Asia, Global Planet. Change 110, 26-39.

806   Maussion F., D. Scherer, T. Mölg, E. Collier, J. Curio and R. Finkelnburg (2014),

807   Precipitation seasonality and variability over the Tibetan Plateau as resolved by the

808   High Asia Reanalysis, J. Climate 27, 1910-1927.

809   Mironov, D., E. Heise, E. Kourzeneva, B. Ritter, N. Schneider, and A. Terzhevik (2010),

810   Implementation of the lake parameterization scheme Flake into the numerical

811   weather prediction model COSMO, Boreal Environ. Res. 15, 218-230.

812   Mischke, S., B. Wünnemann, and E. Appel (2013), Proxies for Quarternary monsoon

813   reconstruction on the Tibetan Plateau, Quart. International 313-314, 1-2.

814   Mitchell T.D., and P.D. Jones (2005), An improved method of constructing a database

815   of monthly climate observations and associated high-resolution grids, Int. J. Climatol.

816   25, 693--712.

817   Molnar, P. (2005), Mio-Pliocene growth of the Tibetan Plateau and evolution of east

818   African climate, Palaeontol. Electronica 8, 1-23.

819   Molnar, P., and B. Rajagopalan (2012), Quaternary Miocene upward and outward

820   growth of eastern Tibet and decreasing monsoon rainfall over the northwestern

821   Indian subcontinent since ~10 MA, Gephys. Res. Lett. 39, L09702.

822   Mutz, S.G., T.A. Ehlers, J. Li, C. Steger, H. Paeth, M. Werner, and C.J. Poulsen (2016),

823   Precipitation d18O over the Himalaya-Tibet orogen from ECHAM5-wiso sImulations:

824   Statistical analysis of temperature, topography, and precipitation. J. Geophys.

825   Res.,121, 9278-9300, doi:10.1002/2016JD024856.

34

Climate
of the Past
Discussions

EGU

826   Netzel P., and T. Stepinski (2016), On using a clustering approach for global climate

827   classification, J. Climate, doi:10.1175/JCLI-D-15-0640.1.

828   Paeth, H. (2011), Postprocessing of simulated precipitation for impact studies in West

829   Africa – Part I: model output statistics for monthly data, Climate Dyn. 36, 1321--1336.

830   Paeth, H., K. Born, R. Girmes, R. Podzun, and D. Jacob (2009), Regional climate

831   change in tropical Africa under greenhouse forcing and land-use changes, J.

832   Climate 22, 114--132.

833   Paeth, H., K. Born, R. Podzun, and D. Jacob (2005), Regional dynamical downscaling

834   over West Africa: Model evaluation and comparison of wet and dry years,

835   Meteorolog. Z. 14, 349--367.

836   Paeth, H., N.M. Hall, M.A. Gaertner, M. Dominguez Alonso, S. Moumouni, J. Polcher,

837   P.M. Ruti, A.H. Fink, M. Gosset, T. Lebel, A.T. Gaye, D.P. Rowell, W. Moufouma-

838   Okia, D. Jacob, B. Rockel, F. Giorgi, and M. Rummukainen (2011), Progress in

839   regional downscaling of West African precipitation, Atmos. Sci. Let. 12, 75--82.

840   Park, H.-S., J.C.H. Chiang, and S. Bordoni (2012), The mechanical impact of the

841   Tibetan Plateau on the seasonal evolution of the South Asian monsoon, J. Climate

842   25, 2394-2407.

843   Paxian, A., and 12 co-authors (2015), Bias reduction in decadal predictions of West

844   African monsoon rainfall using regional climate models, J. Geophys. Res., doi:

845   10.1029/2015JD024143.

846   Polanski, S., A. Rinke, and K. Dethloff (2012), Simulation and comparison between

847   mid-Holocene and preindustrial Indian summer monsoon circulation using a

848   regional climate model, Open Atmos. Sci. J. 6, 42-48.

849   Prell, W.L., and J.E. Kutzbach (1992), Sensitivity of the Indian monsoon to forcing

850   parameters and implications for its evolution, Nature 360, 647-652.

851   Rayner, N.A., E.B. Horton, D.E. Parker, C.K. Folland, and R.B. Hackett (1996), Version

852   2.2 of the global sea ice and sea surface temperature data set, 1903-1994, Clim.

853   Res. Tech. Note CRTN74, Hadley Centre, Bracknell.

854   Ruddiman, W.F. (2014), Earth's climate. Past and Future, W.H. Freeman and

855   Company, New York.

856   Saeed; F., S. Hagemann, and D. Jacob (2011), A framework for the evaluation of the

857   South Asian summer monsoon in a regional climate model applied to REMO, Int..

858   J. Climatol. 32, 430-440.

859   Saraswat, R., R. Nigam, and T. Correge (2013), A glimpse of the Quaternary monsoon

860   history from India and adjoining seas, Palaeogeography, Palaeclimatology,

861   Palaeoecology 397, 1-6.

862   Sein, D.V., U. Mikolajewicz, M. Gröger, I. Fast, W. Cabos, J.G. Pinto, S. Hagemann,

863   T. Semmler, A. Izquierdo, and D. Jacob (2015), Regionally coupled atmosphere-

864   ocean-sea ice-marine biogeochemistry model ROM: 1. Description and validation,

865   J. Adv. Model. Earth Syst. 7, 268–304.

866   Song, J.-H., H.-S. Kang, Y.-H. Byun, and S.-Y. Hong (2009), Effects oft he Tibetan

867   Plateau on the Asian summer monsoon: a numerical case study using a regional

868   climate model, Int. J. Climatol. 30, 743-759.

869   Su, F., X. Duan, D. Chen, and L. Cuo (2013), Evaluation of the global climate models

870   in the CMIP5 over the Tibetan Plateau, J. Climate 26, 3187-3208.

871   Tang, H., A. Micheels, J. Eronen, B. Ahrens, and M. Fortelius (2013a), Asynchronous

872   responses of East Asian and Indian summer monsoons to mountain uplift shown by

873   regional climate modeling experiments, Clim. Dyn. 40, 1531-1549.

874   Tang, H., J. Eronen, A. Micheels, and B. Ahrens (2013b): Strong interannual variation

875   of the Indian summer monsoon in the Quaternary Miocene, Clim. Dyn. 41, 135-153.

36

876   Tapponnier, P., Z.Q. Xu, F. Roger, B. Meyer, N. Arnaud, G. Wittlinger, and J.S. Yang

877   (2991), Oblique stepwise rise and growth oft he Tibet Plateau, Science 294, 1671-

878   1677.

879   Uppala, S., and 45 co-authors (2005), The ERA-40 re-analysis, Q. J. R. Meteorol. Soc.

880   131, 2961-3012.

881   Wang, T., D. Hong, B. Jahn, Y. Tong, Y. Wang, B. Han, and X. Wang (2006), Timing,

882   petrogenesis, and setting of Paleozoic synorogenic intrusions from the Altai

883   mountains, northwest China: Implications for the tectonic evolution of an

884   accretionary orogen, J. Geology 114, 735-751.

885   Werner, M., P.M. Langebroek, T. Carlsen, M. Herold, and G. Lohmann (2011), Stable

886   water isotopes in the ECHAM5 general circulation model: Toward high-resolution

887   isotope modeling on a global scale, J. Geophys. Res. 116, doi:10.1029/2011

888   JD015681.

889   Wilks, D.S. (2006), Statistical methods in the atmospheric sciences, Academic Press,

890   Amsterdam, 627pp.

891   Wu, G., Y. Liu, B. Dong, X. Liang, A. Duan, Q. Bao, and J. Yu (2012): Revisiting Asian

892   monsoon formation and change associated with Tibetan Plateau forcing: I,

893   Formation, Clim. Dyn. 39, 1169-1181.

894   Yang, T., X. Hao, Q. Shao, C.-Y. Xu, C. Zhao, X. Chen, and W. Wang (2012), Multi-

895   model ensemble projections in temperature and precipitation extremes of the

896   Tibetan Plateau in the 21st century, Global Planet. Change 80-81, 1-13.

897   Zhang, R., D. Jiang, Z. Zhang, and E. Yu (2014), The impact of regional uplift oft he

898   Tibetan   Plateau   on   the   Asian   monsoon   climate,   Palaeogeography,

899   Palaeoclimatology, Palaeoecology 417, 137-150.

900   Zheng, Y.Q., G. Yu, S.M. Wang, B. Xue, D.Q. Zhuo, X.M. Zeng, and H.Q. Liu (2004),

901   Simulation of paleoclimate over East Asia at 6 ka BP and 21 ka BP by a regional

902   climate model, Clim. Dyn. 23, 513-529.

903

904   **Figures**
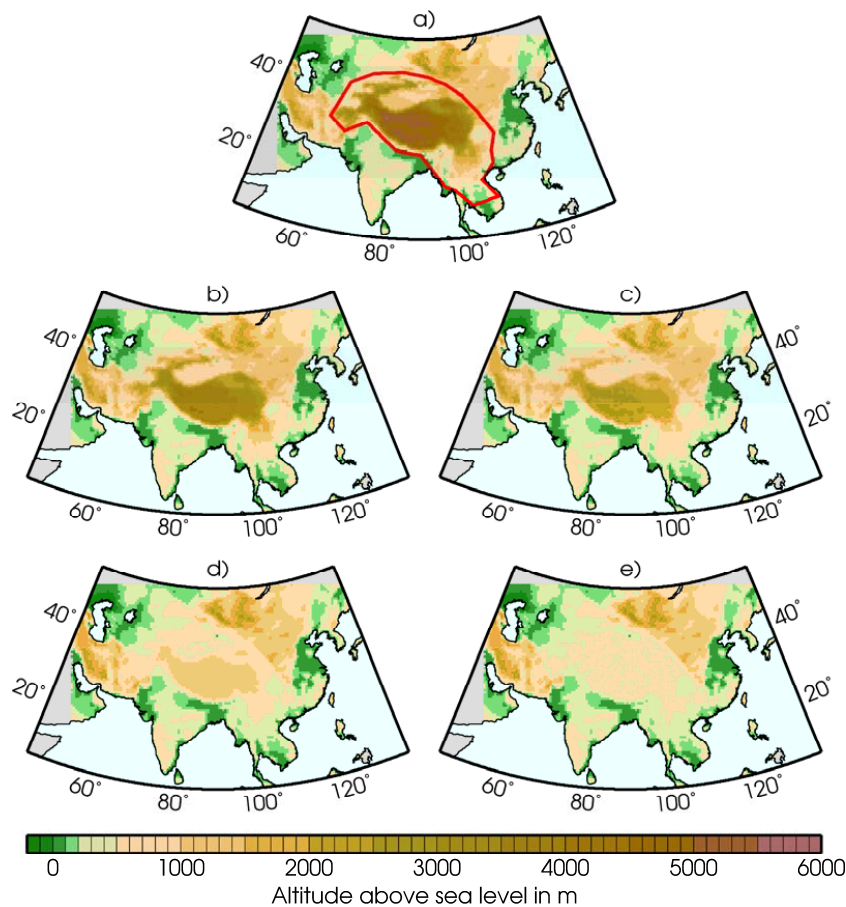
905

906
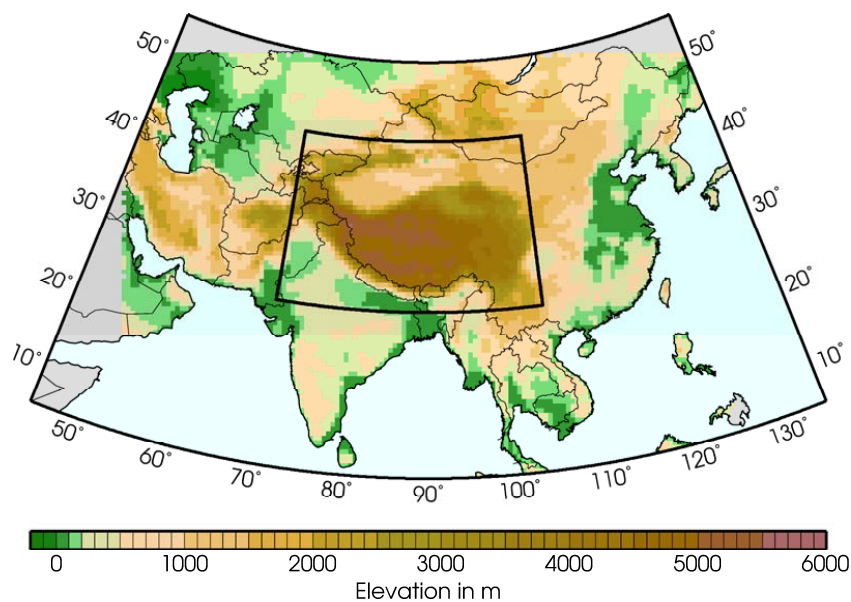
907

908

909   Figure 1: Domain for the dynamical downscaling with REMO (outer region) and for the

910   cluster analysis centered over the Tibetan Plateau (inner region).

911

Climate
of the Past
Discussions
Open Access

912

913

914

915   Figure 2: Topography over Central Asia for the control run with present-day elevation

916   (a) and the stepwise reduction to 75% (b), 50% (c), 25% (d) and complete leveling (e)

917   compared with present-day elevation.

918

Climate
of the Past
Discussions
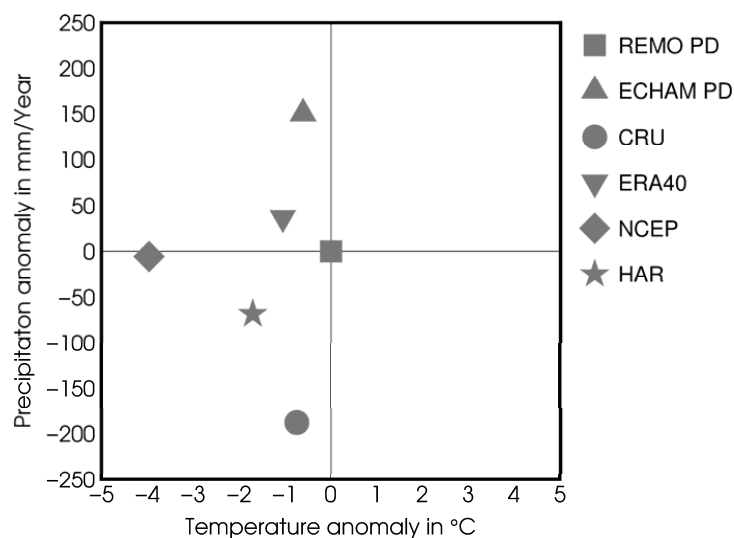
Figure 3: Comparison of mean temperature and precipitation averaged over the cluster domain (cf. Fig. 1) and the time period 1971-2000 from the regional climate model REMO (PD = present-day), the driving global climate model ECHAM, the regional re-analysis HAR, the global reanalysis NCEP, and the CRU observational data set.
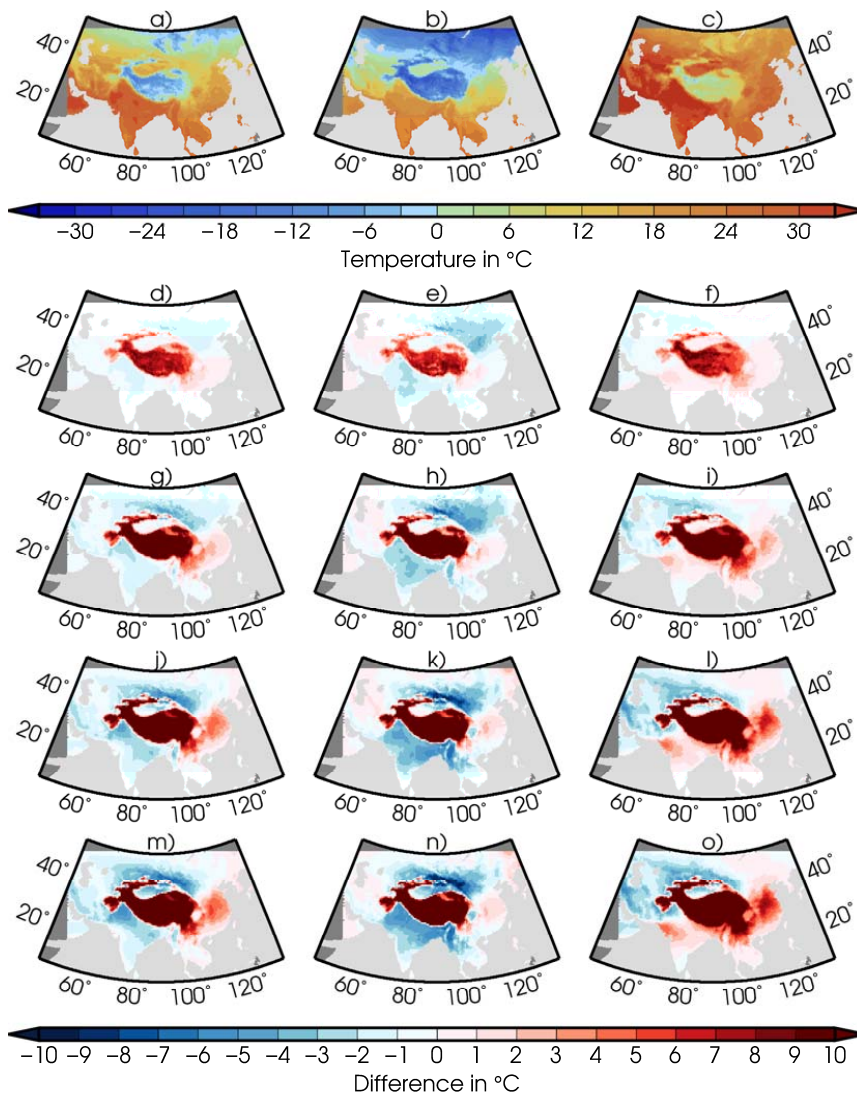
926

927

928 Figure 4: Near-surface temperature averaged over the control period 1971-2000 (top

929 row) for annual means (left column), winter means (middle column) and summer

930 means (right column) as well as temperature changes due to a stepwise reduction of

931 elevation (d-o) from T075 (upper panels) to T000 (lower panels).

932

Climate
of the Past
Discussions

Open Access

EGU

933
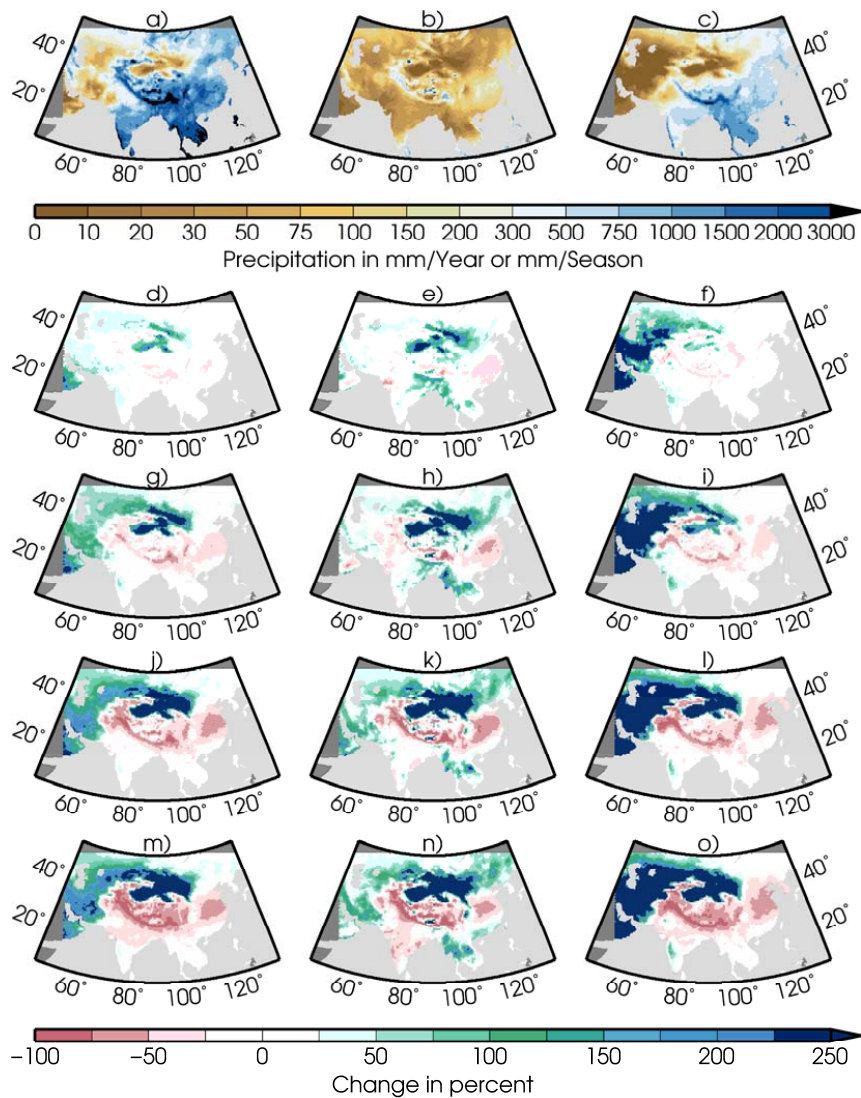
934

935

936   Figure 5: Same as Fig. 4 but for total precipitation.

937

938

939

Climate
of the Past
Discussions
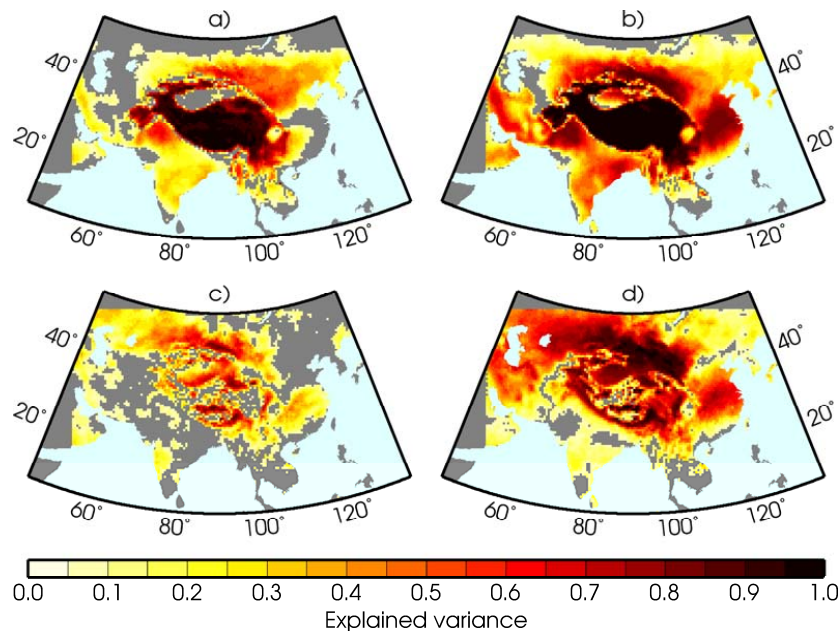
Figure 6: Portion of variance explained by the uplift of the Tibetan Plateau as inferred from a one-way analysis of variance for near-surface temperature (top panels) and total precipitation (bottom panels) assessed between the T100 and T075 experiments (left column) and between all uplift experiments T100 – T000 (right column). Only values significant at the 5% level are plotted.

Climate
of the Past
Discussions
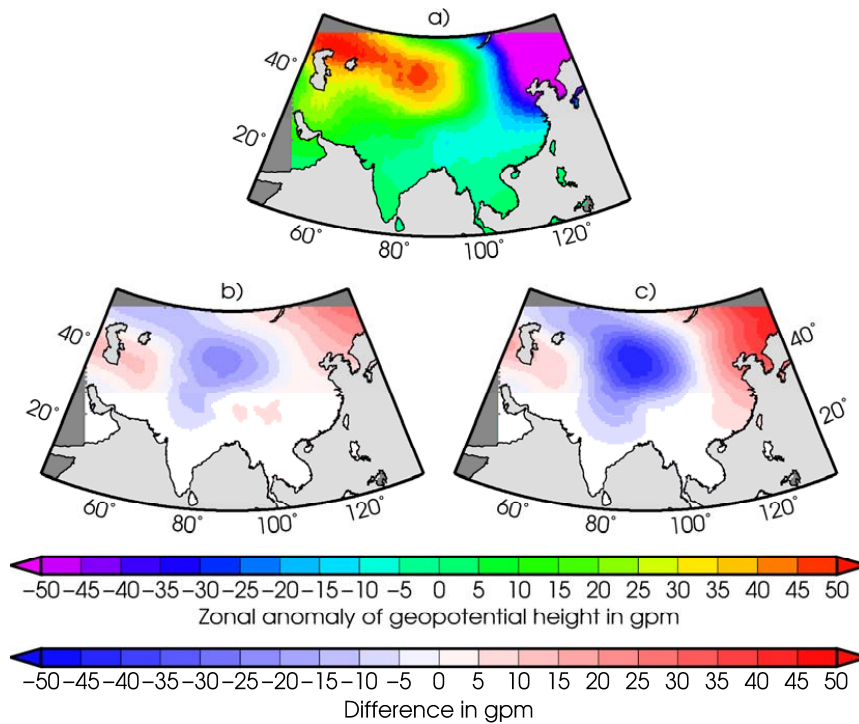
948

949

950   Figure 7: Anomalies of 500 hPa geopotential height from the zonal mean averaged

951   over the control period 1971-2000 (a) and changes due to a stepwise reduction of

952   elevation in the T050 (b) and T000 (c) experiments.

953

45
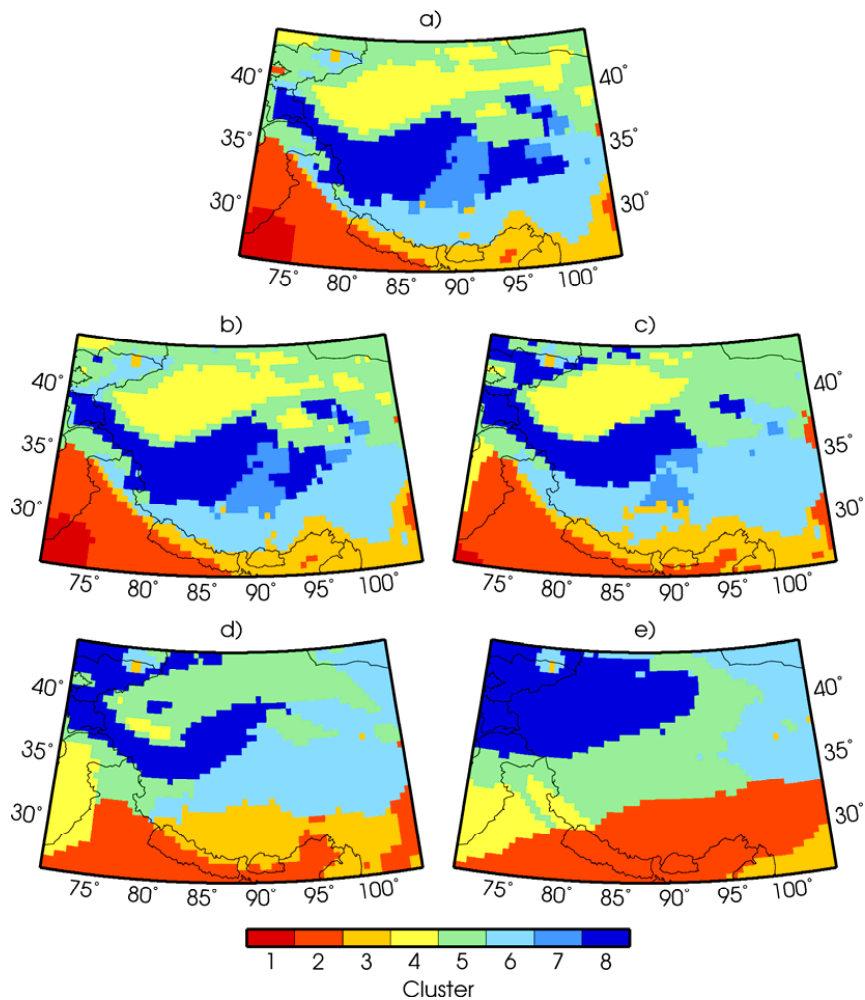
Figure 8: Results of the cluster analysis prescribing 8 clusters in the Tibetan Plateau region for the control period 1971-2000 (a) and projection of the uplift experiments T075 (b) to T000 (e) onto the same centroids from the control period.

Climate
of the Past
Discussions
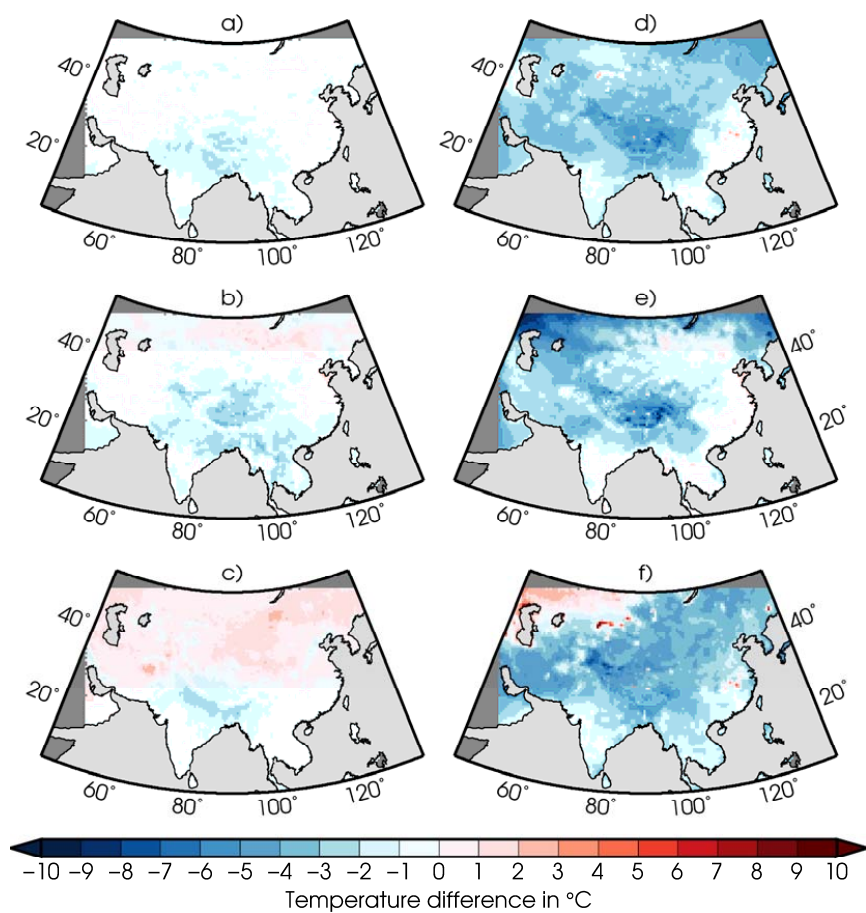
Figure 9: Changes in near-surface temperature for annual means (top row), winter means (middle row) and summer means (bottom row) as simulated by the MH (left column) and LGM (right column) experiment compared with the 1980-1989 control period.
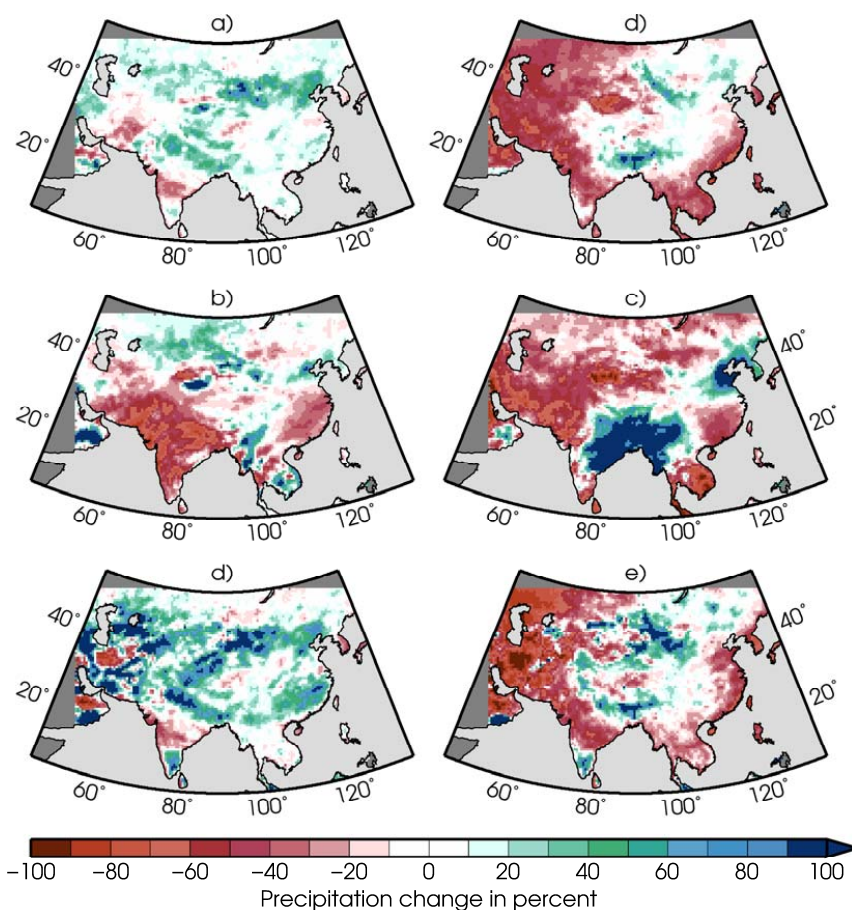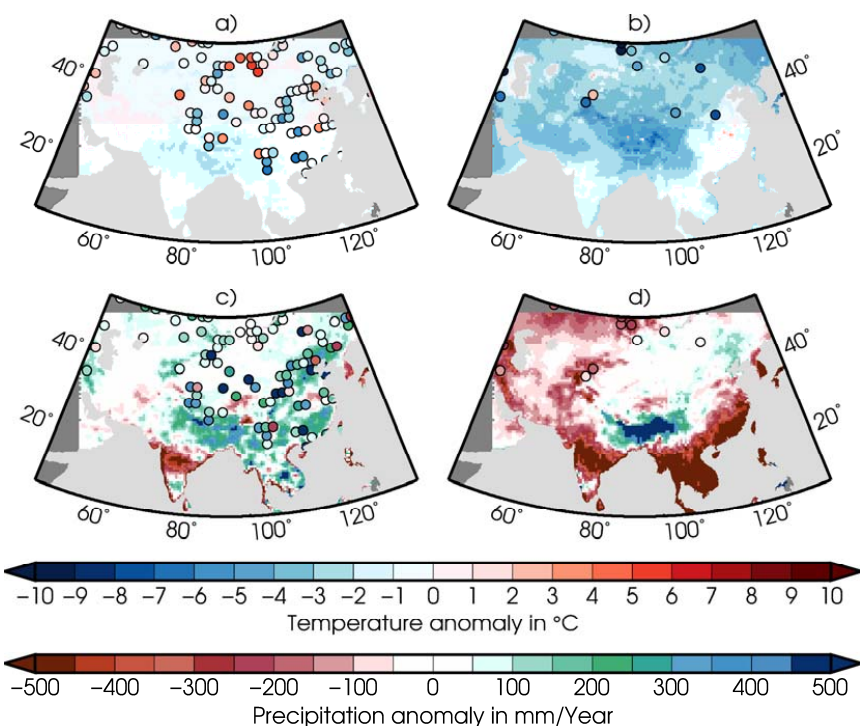
Figure 10: Same as Fig. 9 but for total precipitation.
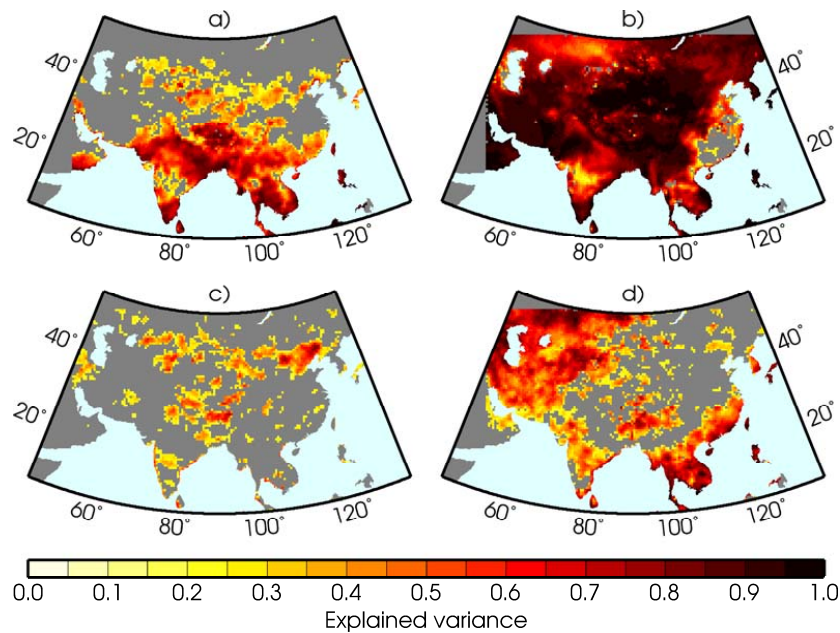
Figure 11: Portion of variance explained by the MH (left column) and LGM (right column) experiment as inferred from a one-way analysis of variance for near-surface temperature (top panels) and total precipitation (bottom panels). Only values significant at the 5% level are plotted.
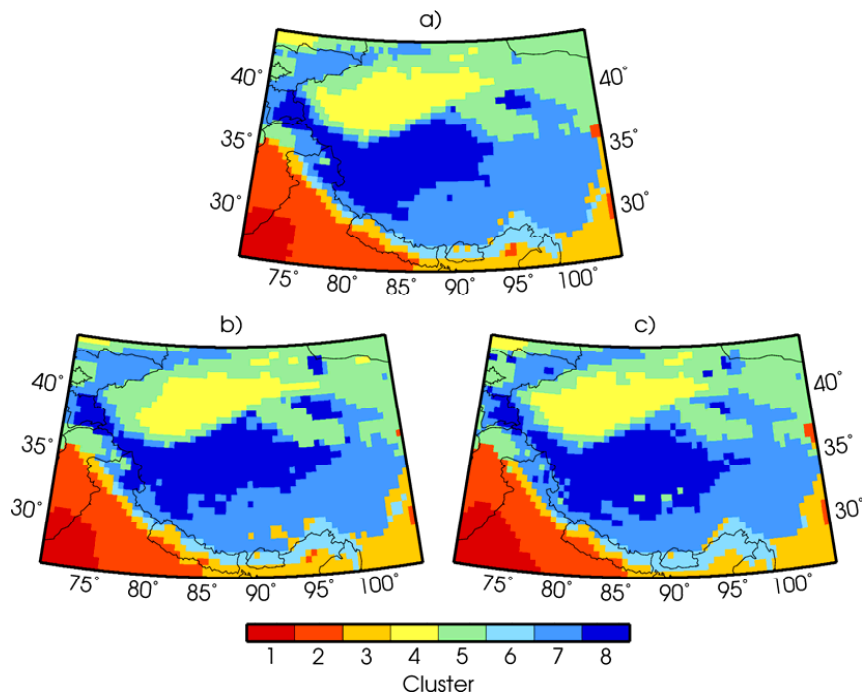
Climate
of the Past
Discussions

Figure 12: Comparison of simulated mean annual temperature (top row) and total pre-

cipitation (bottom row) changes in the MH (left column) and LGM (right column) period

with available paleo-climatic reconstructions (filled circles) from proxy data based on

pollen analysis (Bartlein et al. 2011).

986

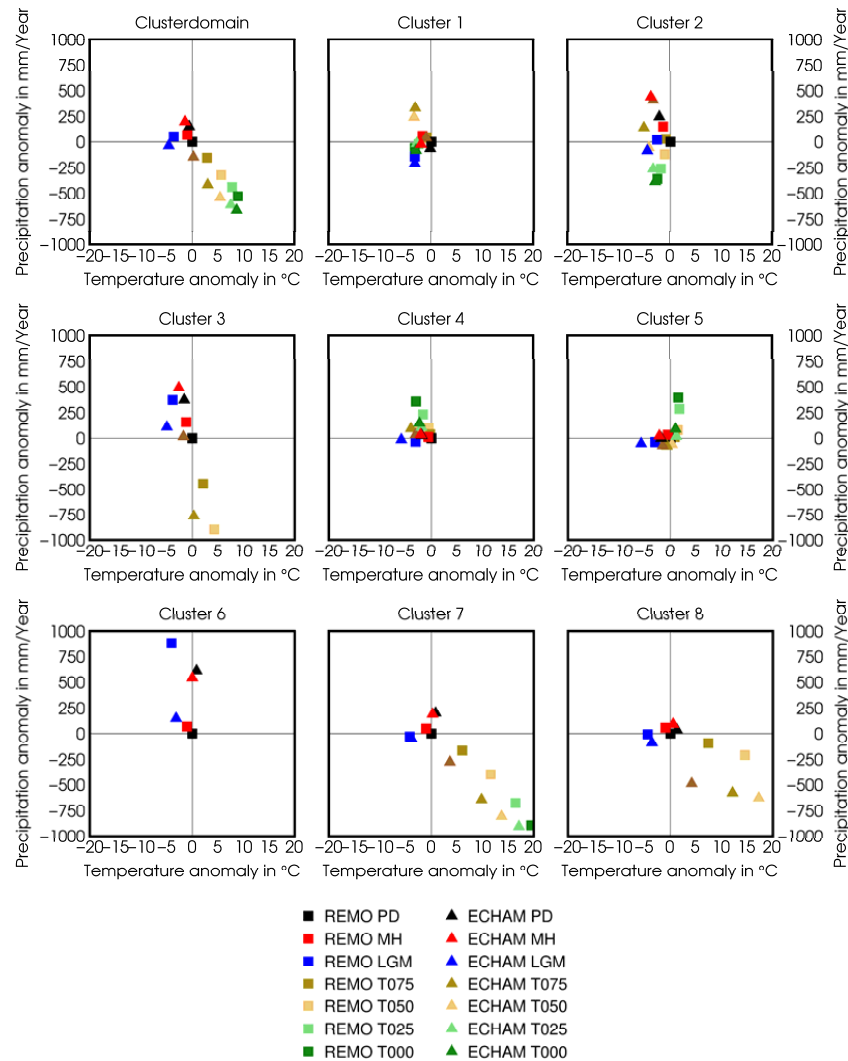Figure 13: Results of the cluster analysis prescribing 8 clusters in the Tibetan Plateau region for the control period 1980-1989 (a) and projection of the MH (b) and LGM (c) experiments onto the same centroids from the control period.

Climate
of the Past
Discussions

Figure 14: Synthesis of changes in annual mean near-surface temperature (x-axis) and total precipitation (y-axis) averaged over the entire cluster domain (top left) and over the individual 8 cluster regions (remaining panels) from the uplift, MH and LGM experiments compared with the respective control periods, once for the regional climate model REMO and once for the driving global climate model ECHAM.